Journal of Computational Physics **179,** 286–312 (2002)
doi:10.1006/jcph.2002.7057

A Conservative Formulation of the Multidimensional Upwind Residual Distribution Schemes for General Nonlinear Conservation Laws

Árpád Csík,*,† Mario Ricchiuto,* and Herman Deconinck*

*Department of Aerospace, Von Karman Institute, St-Genesius-Rode, Belgium; and †Center for Plasma Astrophysics, Katholic University of Leuven, Leuven, Belgium
E-mail: arpi@vki.ac.be

Received July 26, 2001; revised March 5, 2002

In the present paper we consider the numerical solution of systems of general nonlinear hyperbolic conservation laws on unstructured grids by means of the residual distribution method. We propose a new formulation of the first-order linear, optimal positive N scheme, relying on a contour integration of the convective fluxes over the boundaries of an element. Full conservation is achieved for arbitrary flux functions, while the robustness and the monotone shock capturing of the original N scheme is retained. The new variant of the N scheme is combined with the conservative second-order linear *LDA* scheme to obtain a nonlinear second-order monotone B scheme. The performance of the new residual distribution schemes is evaluated on problems governed by the Euler equations. As an application to a more complex system of conservation laws lacking an exact conservative linearization, we solve the ideal magnetohydrodynamics equations in two spatial dimensions.

1. INTRODUCTION

In the last decade a class of multidimensional upwind fluctuation splitting or residual distribution ($\mathcal{RD}$) schemes has emerged for the solution of systems of conservation laws on unstructured grids composed of linear finite elements. The *matrix* variant of the $\mathcal{RD}$ method was developed by van der Weide *et al*. [11] and further improved by Abgrall [1, 2]. It combines Godunow upwinding techniques with compact stencils and space-continuous finite-element methods. Matrix $\mathcal{RD}$ schemes have been used for the numerical approximation of a variety of steady and unsteady flows governed by the Euler or Navier–Stokes equations. Some of the latest developments can be found in [1–7, 10, 14, 18, 19].

0021-9991/02 $35.00

In the framework of the $\mathcal{RD}$ method the existence of a robust *conservative* monotone shock capturing first-order scheme is an essential building block for the development of monotone, second or higher order nonlinear schemes. The N scheme (narrow) [10, 11] is the optimal linear monotone $\mathcal{RD}$ scheme, in the sense that it has the smallest cross-diffusion in its class [15]. Since it operates on the quasilinear form of the governing equations, care has to be taken to maintain the conservative property of this scheme at the discrete level. If the components of the flux vector can be expressed as linear or quadratic functions in terms of a properly chosen parameter vector, then exact conservation of the N scheme can be achieved by applying the Roe–Struijs–Deconinck (RSD) linearization [9]. However, in several other applications, such as the ideal magnetohydrodynamics or the two-phase flow equations, the physics of the problem is described by more complex fluxes or thermodynamics, precluding the simple extension of the RSD linearization. Since the conservation of the convective fluxes is based on a *conservative linearization* in the schemes of van der Weide *et al*. and Abgrall, in this paper we refer to them as *linearization-based residual distribution*, or $\mathcal{LRD}$, schemes.

Csík *et al*. [4, 7] applied the $\mathcal{RD}$ method to the numerical solution of the ideal magnetohydrodynamics (MHD) equations governed by a flux function written as a polynomial of degree three in terms of a specific parameter vector. Since no conservative linearization exists for this system, the authors proposed applying a conservation correction technique involving the computation of the conservation error $\delta\Phi$, given by the difference between the cell residual based on a conservative contour integration and the nonconservative quasilinear form. The conservation error was corrected by distributing $\delta\Phi$ with a central or an appropriate upwind scheme. Although exact conservation was recovered, the resulting monotone schemes lost their intrinsic robustness, especially in terms of convergence.

The problem of discrete conservation in the $\mathcal{RD}$ framework has also been addressed by Abgrall and Barth [2]. They proposed a nonconservative variant of the N scheme in terms of the entropy variables of the system. The nonconservative integrals appearing in the quasilinear form are approximated by an appropriate adaptive quadrature procedure such that the weak solutions are still obtained in the limit of grid refinement. Although the method is computationally more demanding than the original schemes due to the processing of the adaptive quadrature in the entropy variables, it provides a systematic framework for constructing schemes supported by stability analysis via wave decomposition. However, the theory of the method heavily relies on the symmetric formulation of the system. Unfortunately, the ideal MHD equations in strong conservation form are not symmetrizable. In order to obtain the set of symmetrizable ideal MHD equations a nonconservative source term proportional to the divergence of the magnetic field has to be added to the conservative system, rendering the discrete governing equations themselves nonconservative, unless the magnetic field is solenoidal at the discrete level. As a consequence, in the case of ideal MHD the method described in [2] may lead to incorrect jumps accross strong shocks.

In this paper we introduce a new form of the system N scheme of van der Weide *et al*. that guarantees discrete conservation for any nonconservative linearization of the system. While the multidimensional upwinding of the convective residual is still based on the quasilinear form of the governing equations, exact conservation for arbitrary flux functions is incorporated via simple flux contour integrals along element boundaries, such that the underlying robustness and accuracy of the basic schemes is retained. These schemes are referred to as *contour-integration-based residual distribution* or $\mathcal{CRD}$ schemes.

The structure of this paper is the following. In Section two we recall the basic principles of the (*linearization based*) $\mathcal{LRD}$ method for systems of equations in two and three spatial dimensions. The new conservative formulation of the N scheme is described in the third section. In Section four the (*contour integration based*) $\mathcal{CRD}$ method is evaluated for the Euler equations of inviscid gas dynamics. We present computational results containing strong shocks to demonstrate the robustness of the schemes and the monotonicity of the solution. Comparison is made to the results obtained by the $\mathcal{LRD}$ method both for a conservative and nonconservative linearization. In Section five the $\mathcal{CRD}$ method is applied for the solution of the ideal MHD equations to demonstrate its generality. In the last section we give a concluding summary and we point out the potential fields of application of the proposed $\mathcal{CRD}$ approach.

2. RESIDUAL DISTRIBUTION DISCRETIZATION

We consider the numerical solution of a system of q conservation laws in d spatial dimensions,

$$\frac{\partial U}{\partial t} + \nabla \cdot \mathbf{F} = 0, \tag{1}$$

where $U(\mathbf{x}, t)$ is the state vector with q components containing the conserved quantities, $\mathbf{F}(U)$ is the $q \times d$ flux vector with components F_j $(j = 1, \ldots, d)$, and $\mathbf{x}$ is the spatial position vector with coordinates x_j $(j = 1, \ldots, d)$. Writing the Jacobians $A_j = \partial F_j / \partial W$ in terms of a parameter vector $W(U)$ connected to U via transformation $T = \partial U / \partial W$, the quasilinear form of Eq. (1) is

$$T \frac{\partial W}{\partial t} + \sum_{j=1}^{d} \left(A_j \frac{\partial W}{\partial x_j} \right) = 0. \tag{2}$$

In the framework of the $\mathcal{RD}$ method the solution is approximated in the piecewise linear finite-element space over an arbitrary unstructured grid,

$$W^h(\mathbf{x}, t) = \sum_{i=1}^{N} W_i(\mathbf{x_i}, t) \omega_i^h(\mathbf{x}), \tag{3}$$

where N is the total number of nodes in the mesh, $W_i(\mathbf{x_i}, t)$ is the time-dependent nodal value of the solution at node i, and $\omega_i^h(\mathbf{x})$ is the piecewise linear shape function equal to unity at node i and vanishing outside of the elements sharing i as a vertex. Considering the number of degrees of freedom in two and three spatial dimensions, the linear elements are triangles and tetrahedra, respectively.

Integration of Eq. (2) over a linear element E with the approximation W^h yields the definition of the total fluctuation or the cell residual Φ^E in a *discrete* form:

$$\Phi^E = \int_E \sum_{j=1}^{d} \left(A_j \frac{\partial W}{\partial x_j} \right) dV. \tag{4}$$

The construction of the multidimensional upwind $\mathcal{RD}$ schemes requires the cell residual to be approximated in the form

$$\Phi^E = \left[\sum_{j=1}^{d} (\bar{A}_j \hat{\mathbf{x}}_\mathbf{j})\right] \cdot \int_E \nabla W^h \, dV, \tag{5}$$

where $\hat{\mathbf{x}}_\mathbf{j}$ is the unit vector in the jth coordinate direction and $\bar{A}_j = A_j(\bar{W})$ is the analytic Jacobian taken in an averaged state $\bar{W}$. In smooth flows the quasilinear form (5) can be used without additional constraints to give a proper description of the flow field. However, if the solution is discontinous, conservation of the cell residual is an additional constraint in order to obtain proper jumps accross discontinuities, as discussed in Section 2.2.

Since W^h has linear variation in element E by assumption (3), exact evaluation of the integral term in Eq. (5) yields

$$\Phi^E = \left[\sum_{j=1}^{d} (\bar{A}_j \hat{\mathbf{x}}_\mathbf{j})\right] \cdot \frac{1}{d} \sum_{i=1, i\in E}^{d+1} W_i \mathbf{n}_\mathbf{i} = \sum_{i=1, i\in E}^{d+1} K_i W_i, \tag{6}$$

where $\mathbf{n}_\mathbf{i}$ is the inward-pointing normal vector of the face opposite to i, scaled with the area of the face, and index i goes through the local nodes of the element. Matrix K_i is the following linear combination of the Jacobians:

$$K_i = \frac{1}{d}\left[\sum_{j=1}^{d} (\bar{A}_j \hat{\mathbf{x}}_\mathbf{j})\right] \cdot \mathbf{n}_\mathbf{i}, \quad \bar{A}_j = A_j(\bar{W}). \tag{7}$$

Due to the hyperbolic nature of the governing Eq. (1), matrix K_i has q real eigenvalues and a complete set of linearly independent eigenvectors. Diagonalization of matrix K_i yields

$$K_i = R_i \Lambda_i L_i, \tag{8}$$

where the columns of R_i are the right eigenvectors, $L_i = R_i^{-1}$, and Λ_i is a diagonal matrix containing the eigenvalues of K_i. Introducing $\Lambda_i^{\pm} = (\Lambda_i \pm |\Lambda_i|)/2$, the so-called multidimensional upwind parameters are defined as

$$K_i^+ = R_i \Lambda_i^+ L_i \quad \text{and} \quad K_i^- = R_i \Lambda_i^- L_i. \tag{9}$$

Following the solution procedure of the $\mathcal{RD}$ approach, Φ^E is decomposed in all of the elements into subresiduals which are distributed to the nodes of E. The distribution function Φ_i^E defines the subresidual, i.e., the fraction of the total cell residual distributed to node i in element E. For consistency it is required that the sum of the distribution functions in an element be the total cell residual Φ^E:

$$\Phi^E = \sum_{i=1, i\in E}^{d+1} \Phi_i^E. \tag{10}$$

The multidimensional upwind property of the $\mathcal{RD}$ schemes implies that no residual is sent to node i in element E if all the eigenvalues of the local matrix K_i are nonpositive [10, 11]; i.e.,

$$\Phi_i^E = \vec{0} \quad \text{if } K_i^+ = \hat{0}, \tag{11}$$

where $\vec{0}$ and $\hat{0}$ stand for the null vector and null matrix, respectively. Assembling all of the contributions Φ_i^E from the elements to the nodes, the semidiscrete form of the governing equation at node i takes the form

$$\frac{dU_i}{dt} = -\frac{1}{V_i} \sum_{E, i \in E} \Phi_i^E, \tag{12}$$

where V_i is the volume of the median dual of node i equal to $1/(d+1)$ times the total volume of all the linear elements sharing node i as a vertex.

The simple explicit forward Euler discretization of the temporal derivative at node i leads to the following discrete equation:

$$U_i^{n+1} = U_i^n - \frac{\Delta t_i}{V_i} \sum_{E, i \in E} \Phi_i^E. \tag{13}$$

In the update scheme (13) superscripts n and $n+1$ label the solution at the corresponding time levels and Δt_i is the local time step at node i limited by considerations of positivity and stability. First-order temporal accuracy can be achieved by global time stepping; i.e. $\Delta t_i = \Delta t$ for $\forall i = 1, \ldots, N$, where $\Delta t = \min(\Delta t_k)_{k=1,\ldots,N}$. For steady state problems the accuracy of the transient solution is not a concern; therefore local time stepping is applied to accelerate the iterative procedure.

The definition of Φ_i^E determines the properties of different $\mathcal{RD}$ schemes. Important design principles are *positivity* ($\mathcal{P}$) and *linearity preservation* ($\mathcal{LP}$). In practical computations a $\mathcal{P}$ scheme captures shocks in a monotonic manner, while $\mathcal{LP}$ schemes produce a second-order-accurate solution in steady smooth flows [1, 4, 7, 10]. In this paper we consider a linear $\mathcal{P}$ scheme, a linear $\mathcal{LP}$ scheme, and a nonlinear $\mathcal{P}$ and $\mathcal{LP}$ scheme, which is obtained by applying a blending of the distribution functions of the linear $\mathcal{P}$ and $\mathcal{LP}$ schemes. Some more details on property $\mathcal{P}$ are given in Section 2.1.

2.1. Positivity of the $\mathcal{RD}$ Schemes

An important design criterion in the construction of numerical discretization techniques is the ability of the schemes to produce monotone solutions across discontinuities and steep gradients in the sense that spurious oscillations are not generated in the pre- and postshock domains. In the context of cell vertex $\mathcal{RD}$ schemes the concept of positivity ($\mathcal{P}$) has been considered as a generalization of the TVD principles for Godunov schemes to unstructured grids composed of linear finite elements. The notion of positivity as a monotonicity concept has also been used in a pure finite-volume context, where it is known as the LED (local extremum diminishing) property [13].

Let us consider a scalar conservation law, with u_j^n being the unknown nodal quantity at time level n. New extrema are not generated by the scheme if the discrete solution at level $n+1$ is obtained as a convex sum of the solution at level n on a compact stencil surrounding node j:

$$u_j^{n+1} = \sum_{i=1}^{N} \alpha_i u_i^n, \quad \text{where } 0 \le \alpha_i \le 1 \text{ and } \sum_{i=1}^{N} \alpha_i = 1. \tag{14}$$

The class of $\mathcal{RD}$ schemes satisfying Eq. (14) under a CFL type condition is called *positive*. The concept of monotonicity based on positivity or LED is valid for scalar equations only. For systems of equations a relatively simple intuitive extension of the corresponding scalar conditions is maintained in practice, leading to the system variant of the schemes, which yield oscillation-free results [1, 10, 11]. Recently, Abgrall and Barth [2] showed satisfaction of a *discrete entropy inequality* for a nonconservative variant of the system N scheme of van der Weide *et al*. [11], retaining the correct weak solutions in the limit of mesh refinement under certain assumptions. The authors show that their scheme can be used for general first-order conservation laws equipped with an entropy inequality.

2.2. Conservation and Roe–Struijs–Deconinck Linearization

Equation (4) can be equivalently written in the form of a conservative contour integral along the boundary ∂E of the element by using Gauss' theorem,

$$\Phi^E = \oint_{\partial E} \mathbf{F}(W^h) \cdot \mathbf{n}\, dS, \tag{15}$$

where $\mathbf{n}$ is the outward-pointing unit normal vector of surface element dS. In order to capture shocks with proper jump relations, the underlying discretization of Φ^E has to be conservative; i.e., at the discrete level it has to be equivalent to the computation of the contour integral of the fluxes along the boundaries ∂E of element E according to a chosen integration rule in Eq. (15). This property is essential for canceling internal fluxes if Eq. (12) is summed up for all of the nodes. The standard way to achieve the conservation of the fluxes is to define an appropriate averaged state $\bar{W}$ such that Eqs. (15) and (5) yield identical approximation of Φ^E. This procedure is called *conservative linearization* and the corresponding conservative schemes are the *linearization-based residual distribution*, or $\mathcal{LRD}$, schemes.

The main difficulty in the solution procedure of general nonlinear conservation laws by the $\mathcal{LRD}$ method lies in the fact that the construction of $\mathcal{P}$ schemes requires the eigenvalue decomposition of the quasilinear form, and hence it strongly relies on the existence of a conservative linearization. In general it is not possible to generate a constant state $\bar{W}$ such that Eqs. (5) and (15) are identical at the discrete level. Indeed, this implies

$$\bar{A}_j = A_j(\bar{W}) = \frac{1}{V^E} \int_E A_j(W^h)\, dV, \quad \forall j \in [1, \ldots, d], \tag{16}$$

where V^E is the volume of element E. Only when the components of the flux vector $\mathbf{F}$ are at most quadratic functions of a properly chosen parameter vector W does the Roe–Struijs–Deconinck (RSD) linearization [9] gives exact satisfaction of Eq. (16), thus preserving exact conservation of the convective fluxes. In this case the corresponding linearized state $\bar{W}$ is a simple arithmetic average of the nodal values:

$$\bar{W} = \frac{1}{d+1} \sum_{i=1, i\in E}^{d+1} W_i. \tag{17}$$

2.3. The Linear *N* Scheme

The linear N scheme (narrow) satisfies the system generalization of property $\mathcal{P}$ [1, 11]. It resolves discontinuities in a monotonic manner and its accuracy is at most first order. The distribution function of the N scheme is

$$\Phi_i^N = K_i^+(W_i - W_{in}), \quad K_i^+ = K_i^+(\bar{W}). \tag{18}$$

State W_{in} is defined by

$$W_{in} = \hat{N} \sum_{i=1, i\in E}^{d+1} K_i^- W_i, \quad K_i^- = K_i^-(\bar{W}), \tag{19}$$

where

$$\hat{N} = \left(\sum_{i=1, i\in E}^{d+1} K_i^- \right)^{-1}, \quad K_i^- = K_i^-(\bar{W}). \tag{20}$$

The inverse matrix $\hat{N}$ does not exist in certain cases, e.g., when the Euler equations are linearized in state $\bar{W}$ corresponding to a stagnation point. However in Ref. [1] it is proven that for a linearized symmetrizable system, $K_i^+\hat{N}$ always has meaning and the N scheme is always well defined. Substituting expression (18) into constraint (10), we obtain

$$\sum_{i=1, i\in E}^{d+1} \Phi_i^N = \sum_{i=1, i\in E}^{d+1} K_i W_i, \quad K_i = K_i(\bar{W}), \tag{21}$$

indicating that the $\mathcal{LRD}$ form of the N scheme is conservative only if the linearized state $\bar{W}$ satisfies Eq. (16).

2.4. The Linear *LDA* Scheme

The distribution functions corresponding to the linear nonmonotone $\mathcal{LP}$ schemes can be cast into the compact form

$$\Phi_i^E = \beta_i^E \Phi^E, \tag{22}$$

where β_i^E is the cell-wise constant distribution matrix satisfying

$$\sum_{i=1, i\in E}^{d+1} \beta_i^E = \hat{I}, \tag{23}$$

with $\hat{I}$ being the unit matrix. If Φ^E is computed independently of β_i^E by using an appropriate conservative contour integration of the fluxes, satisfaction of constraint (23) guarantees the conservative property of the linear $\mathcal{LP}$ schemes for any choice of the linearized state $\bar{W}$.

The *LDA* scheme (low-diffusion A) with property $\mathcal{LP}$ is defined by

$$\beta_i^{LDA} = -K_i^+\hat{N}, \quad K_i^+ = K_i^+(\bar{W}), \tag{24}$$

where matrices K_i^+ and $\hat{N}$ can be computed by using any linearization.

We note that the accuracy of any $\mathcal{RD}$ scheme satisfying property $\mathcal{LP}$ (such as the *LDA* scheme) can be increased to third order [3, 14, 18, 19] by performing a more accurate approximation of the cell residual based on a nonlinear finite-element representation of the solution.

Just like the N scheme, the *LDA* scheme is well posed for linearized symmetrizable systems even if matrix $\hat{N}$ does not exist [1].

2.5. The Nonlinear *B* Scheme

A practical high-resolution scheme has to be both monotone ($\mathcal{P}$) and at least second order ($\mathcal{LP}$). Such a scheme is necessarily nonlinear [20] and can be obtained by applying a proper blending of the distribution functions of a linear $\mathcal{P}$ and $\mathcal{LP}$ scheme. The distribution function of the B scheme (blended) is defined as

$$\Phi_i^B = \hat{\Theta}\Phi_i^N + (\hat{I} - \hat{\Theta})\Phi_i^{LDA}, \tag{25}$$

where $\hat{\Theta}$ is a diagonal nonlinear blending matrix [1, 4, 7, 10] given by

$$\Theta_{k,k} = \frac{\left|\Phi_k^E\right|}{\sum_{j=1, j\in E}^{d+1} \left|\Phi_{j,k}^N\right|}. \tag{26}$$

In expression (26) index $k = [1, \ldots, q]$ refers to the kth equation of the system; i.e., Φ_k^E and $\Phi_{j,k}^N$ are the kth component of vectors Φ^E and Φ_j^N, respectively. If the linear $\mathcal{P}$ and $\mathcal{LP}$ schemes are conservative, then the B scheme satisfies Eqs. (15) and (10), justifying the importance of a conservative N scheme. We note that other definitions of the blending matrix exist, e.g., based on the considerations of entropy stability proposed by Abgrall [1].

3. CONSERVATIVE CONTOUR-INTEGRATION-BASED *N* SCHEME

In order to construct a conservative form of the N scheme for general nonlinear conservation laws, we propose to replace Eq. (19) for the computation of state W_{in} by the expression

$$W_{in} = -\hat{N}\left(\sum_{i=1, i\in E}^{d+1} K_i^+ W_i - \Phi^E\right), \quad K_i^+ = K_i^+(\bar{W}), \tag{27}$$

where Φ^E is the cell residual computed in a conservative manner according to a chosen integration rule in Eq. (15) while K_i^+ and $\hat{N}$ are based on any choice of the linearized state $\bar{W}$. By summing up Eq. (18) over the nodes of the cell, it is straightforward to verify that the resulting N scheme is conservative according to Eqs. (15) and (10). In practice Φ^E is calculated from Eq. (15) either approximately by Simpson's rule or exactly, based on assumption (3).

In principle, state $\bar{W}$ can be defined by any linearization, since it is only used for the approximate multidimensional upwinding of the convective residual Φ^E. Thus, in practice we follow considerations of simplicity and efficiency. If an exact RSD linearization is applied for a given flux vector $\mathbf{F}$ in terms of parameter vector W, then Eq. (27) reduces to (19).

Since the conservative property of the new form of the N scheme is based on the contour integration of the fluxes along the boundary of an element, we refer to this formulation as the *contour-integral-based residual distribution*, or $\mathcal{CRD}$, version of the N scheme.

Just as in the case of the standard $\mathcal{LRD}$ N scheme combined with RSD linearization, exact positivity of the components of the solution W obtained by the new $\mathcal{CRD}$ N scheme cannot be proven. However, its close formal relation to the original schemes indicates that the satisfaction of a CFL-condition-based time-step limitation yields oscillation-free solutions across discontinuities while preserving the extreme robustness and monotonicity of the original $\mathcal{LRD}$ N scheme. Indeed, in Section 4 we present numerical experiments to demonstrate that all the positive $\mathcal{CRD}$ schemes based on a nonconservative linearization and definition (27) retain monotone shock capturing property in the presence of strong steady and unsteady shocks.

4. NUMERICAL RESULTS FOR THE EULER EQUATIONS

In order to demonstrate the robustness and the monotone shock capturing of the $\mathcal{CRD}$ schemes based on the new formulation of the N scheme, we present several test computations containing strong steady and unsteady shocks in two spatial dimensions. First we evaluate the performance of the $\mathcal{CRD}$ schemes by solving the Euler equation

$$\frac{\partial}{\partial t}\begin{pmatrix}\rho\\ \rho\mathbf{v}\\ E\end{pmatrix}+\nabla\cdot\begin{pmatrix}\rho\mathbf{v}\\ \rho\mathbf{v}\mathbf{v}+\hat{I}\,p\\ \mathbf{v}(E+p)\end{pmatrix}=0, \tag{28}$$

where ρ is the fluid density, $\mathbf{v}$ is the velocity vector, p is the thermal pressure, and E is the total energy density defined by

$$E=\frac{p}{\gamma-1}+\frac{1}{2}\rho\mathbf{v}\cdot\mathbf{v}. \tag{29}$$

For the Euler equations the conservative RSD linearization [9] is based on the Roe parameter vector:

$$W=\sqrt{\rho}[1,v_x,v_y,(E+p)/\rho]^T \quad\text{and}\quad \bar{W}=\frac{1}{d+1}\sum_{j=1,j\in E}^{d+1}W_j. \tag{30}$$

In the $\mathcal{CRD}$ schemes the linearization of the Jacobians can be done in any set of variables, and in the present results the following set of primitive variables is employed:

$$P_{\text{Euler}}=[\rho,v_x,v_y,p]^T. \tag{31}$$

As a consequence of this choice, matrices K_i are always diagonalizable with real eigenvalues in the mean state $\bar{P}$ if the pressure and density are positive at all of the vertices of the element involved in the linearization.

The reference solution for the steady Euler equations is computed by the $\mathcal{LRD}$ schemes based on the existing RSD linearization, which is conservative and positive by construction. We also show the nonconservative solution for the N scheme obtained by the linearization done in the primitive variables (31) in combination with the original definition (19) of W_{in}.

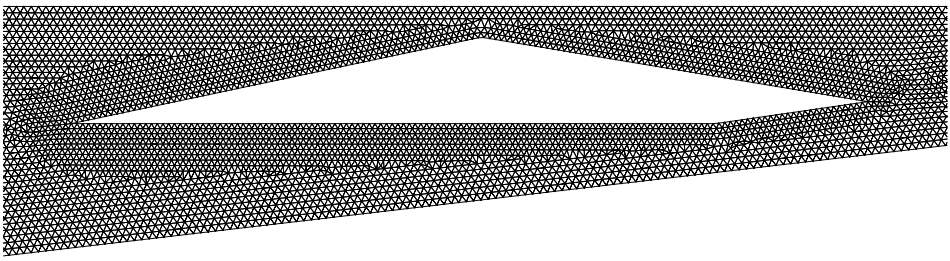

FIG. 1. Part of the unstructured grid used in the scramjet computation. The full grid contains 7,056 nodes and 13,383 elements.

The value of the ratio of specific heats is $\gamma = 1.4$ and $5/3$ in the steady and unsteady computations, respectively.

4.1. Scramjet Inlet

In this problem we consider a flow field involving steady oblique reflecting shocks. At the supersonic inlet of the scramjet the Mach number is $M = 3.6$, the top boundary corresponds to a symmetry line, the bottom boundary consists of an inviscid wall, and the outlet flow at the right is still supersonic. The geometry of the grid is the same as the one used in Ref. [15]. Figure 1 shows a detail of the mesh containing 7,056 nodes and 13,383 elements in total.

The solution computed by the $\mathcal{CRD}$ N scheme and B scheme based on the linearization in the primitive variables (31) is given in Fig. 2. Both solutions show a good prediction of the compression of the flow through the series of shocks reflecting between the symmetry line and the wedge. The higher resolution of the B scheme is clear, while both solutions are monotone. The distribution of Mach number and pressure along the symmetry line is shown in Figs. 3 and 4. The solid line and the symbols correspond to the reference solution (original $\mathcal{LRD}$ scheme with RSD linearization) and the numerical values obtained by the

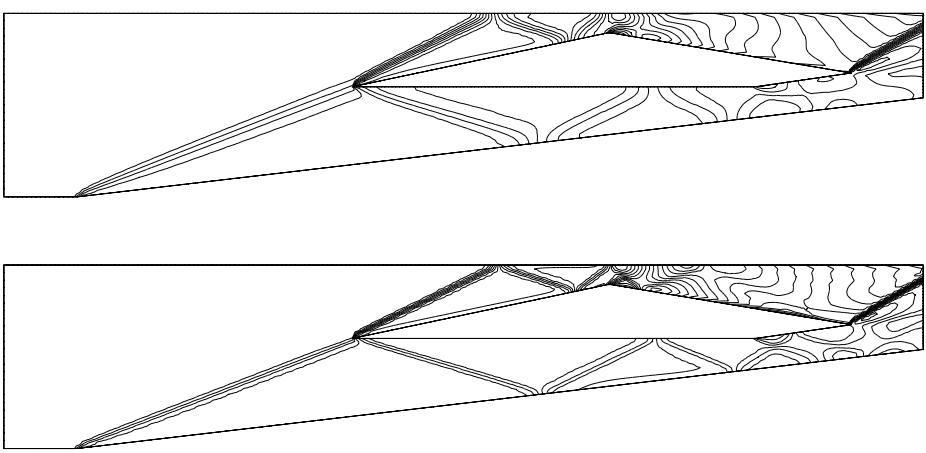

FIG. 2. Mach number contour lines in the scramjet computed by the first-order $\mathcal{CRD}$ N scheme (top) and the second-order $\mathcal{CRD}$ B scheme (bottom).

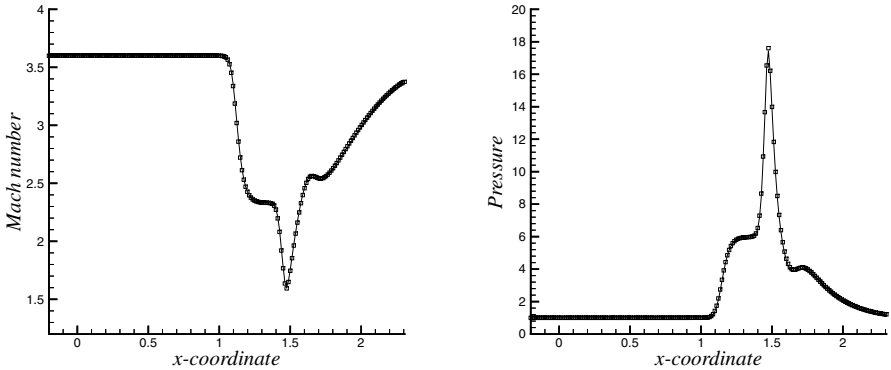

FIG. 3. Mach number and pressure along the symmetry axes of the scramjet computed by the first-order N scheme. Solid lines and symbols correspond to the reference $\mathcal{LRD}$ and the new $\mathcal{CRD}$ method, respectively.

new $\mathcal{CRD}$ schemes, respectively. One can observe that the squares match the solid line closely without spurious oscillations, showing that the new approach without the RSD linearization produces results almost identical to the reference solution.

In Fig. 5 the convergence histories corresponding to all four computations are presented. The logarithm of

$$\|\Delta\rho\|_2 = \sqrt{\frac{\sum_{i=1}^{N}(\Delta\rho_i)^2}{N}} \tag{32}$$

is plotted versus the number of forward Euler explicit iterations combined with local time stepping. Quantity $\Delta\rho_i = \rho_i^{n+1} - \rho_i^n$ is the actual change in the density at node i between time steps n and $n+1$. On this problem the $\mathcal{LRD}$ and $\mathcal{CRD}$ N schemes converge with the same rate to the steady state up to machine accuracy. The convergence histories are practicaly identical; the small differences are not visible on the resolution of the plot. The nonlinear B schemes converge at approximately three orders of magnitude and then end up in limit cycling. The $\mathcal{CRD}$ B scheme converges slightly less than the $\mathcal{LRD}$ B scheme. The relatively poor convergence is a particular feature of present nonlinear $\mathcal{RD}$ schemes (such as the B

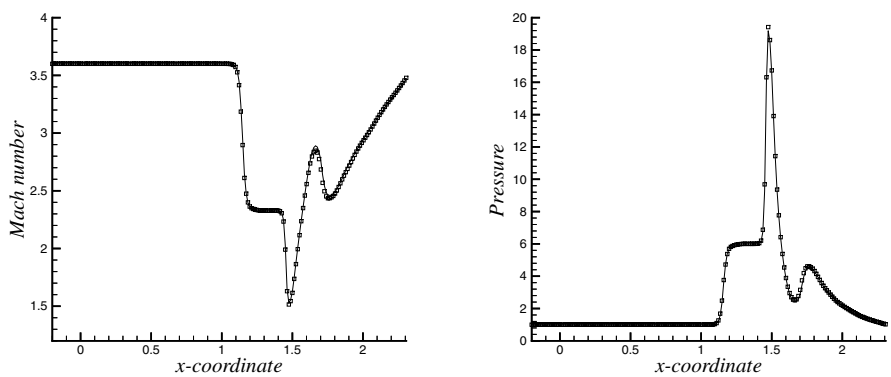

FIG. 4. Mach number and pressure along the symmetry axes of the scramjet computed by the second-order B scheme. Solid lines and symbols correspond to the reference $\mathcal{LRD}$ and the new $\mathcal{CRD}$ method, respectively.

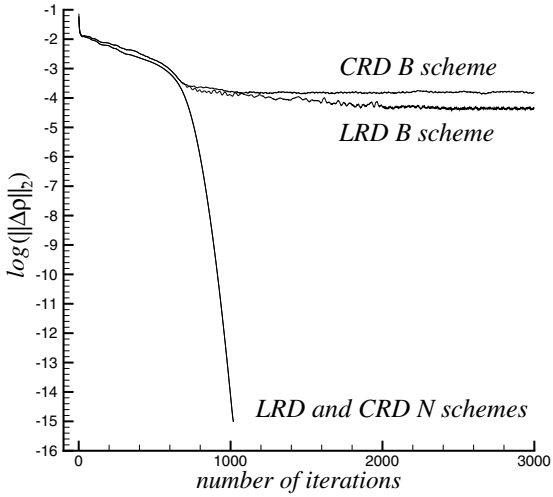

FIG. 5. Convergence histories corresponding to the computations of the flow field in a scramjet. Results are obtained by the first-order $\mathcal{LRD}$ and $\mathcal{CRD}$ N schemes and the second-order $\mathcal{LRD}$ and $\mathcal{CRD}$ B schemes.

scheme), reported by other authors as well [1]. Nevertheless, the computations demonstrate that the $\mathcal{CRD}$ apprach does not change the qualitative behavior of the convergence rate of the $\mathcal{LRD}$ schemes.

4.2. Mach 10 Bow Shock around a Cylinder

In order to test the robustness of the $\mathcal{CRD}$ N scheme in the presence of a strong discontinuity, we perform the test case of a steady Mach 10 bow shock flow around a cylinder. The Delaunay mesh contains 12,085 nodes and 23,740 elements. Due to reasons of symmetry the flow field is computed over the upper left quadrant of the cylinder only.

Mach number and pressure contour lines are plotted in Fig. 6. The solution is clean and free of wiggles in both quantities, despite of the presence of the strong normal shock across the stagnation line. The same computation was performed by the $\mathcal{LRD}$ N scheme based on the RSD linearization, and the contour lines matched so well that on the plots it was almost impossible to distinguish the two computations. The only difference appeared on the Mach number contour plots close to the stagnation line, where the $\mathcal{LRD}$ solution was slightly more wiggly right after the normal shock.

In Fig. 7 we show the Mach number and pressure (symbols) along the stagnation line obtained by the new conservative $\mathcal{CRD}$ scheme (left column) and by the standard $\mathcal{LRD}$ scheme based on the nonconservative linearization in primitive variables (right column). The solid line represents the reference solution. The $\mathcal{CRD}$ results match the reference line with a high accuracy, indicating that the excellent robustness and monotonicity of the conservative $\mathcal{LRD}$ N scheme are retained by the new $\mathcal{CRD}$ N scheme. The plots demonstrate that the linearization can be done in primitive variables if state W_{in} is based on the new formula (27) in the definition of the N scheme. However, the nonconservative nature of the primitive linearization in combination with the standard scheme (19) is confirmed by the wrong shock position and shock strength shown on the right of Fig. 7.

The convergence histories corresponding to the $\mathcal{LRD}$ and $\mathcal{CRD}$ N schemes are plotted in Fig. 8. In the first period of the computation the convergence of the two schemes are very

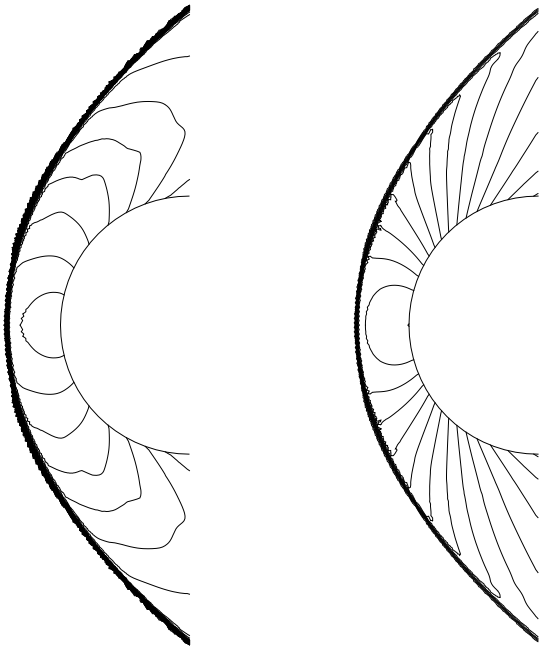

FIG. 6. Mach 10 bow shock flow around a cylinder computed by the first-order $\mathcal{CRD}$ N scheme. Mach number (left) and pressure (right) contour lines are shown.

close to each other. After the bow shock is in position and the solution starts to converge in the postshock regime a small offset develops between the curves. Both the $\mathcal{LRD}$ and the $\mathcal{CRD}$ N schemes reach the level of machine accuracy, illustrating the robust convergence of the new formulation.

The computation of the same bow shock flow was performed by the $\mathcal{LRD}$ and $\mathcal{CRD}$ B schemes as well. Although the schemes kept both the density and the pressure positive, the level of limit cycling was inadequately high, expressing the need for a significantly improved robust nonlinear second-order positive scheme in the framework of the $\mathcal{RD}$ method.

4.3. Contact Discontinuity

An undesired feature of the standard $\mathcal{LRD}$ method based on the RSD linearization is that the solution of shear flows can be inaccurate and even unstable under certain conditions. The reason is due to the special choice of the Roe variable $(E + p)/\sqrt{\rho}$. In the case of a shear flow the pressure gradient vanishes, as does the corresponding force in the momentum equation. However, if the distribution of the residual is based on the Roe variables, then $\nabla[(E + p)/\sqrt{\rho}] \neq 0$ in an element spreading across the shear; thus the schemes may detect a pressure gradient. This effect is the most pronounced when a grid-aligned contact discontinuity has to be resolved on a structured triangulation of the domain.

To illustrate this problem, we perform the numerical computation of a steady contact discontinuity over a computational domain forming a rectangle ($-1 \leq x \leq 1$ and $-0.5 \leq y \leq 0.5$). The discontinuity propagates through the center of the structured diamond mesh, parallel to the y-axes (see Fig. 9). In the initial state $\rho = 1$, $p = 1$, $v_x = 0$ everywhere, while $v_y = 4$ for $x \leq 0$ and $v_y = 8$ for $x > 0$. At the bottom and top boundaries supersonic inlet and outlet conditions are imposed, respectively.

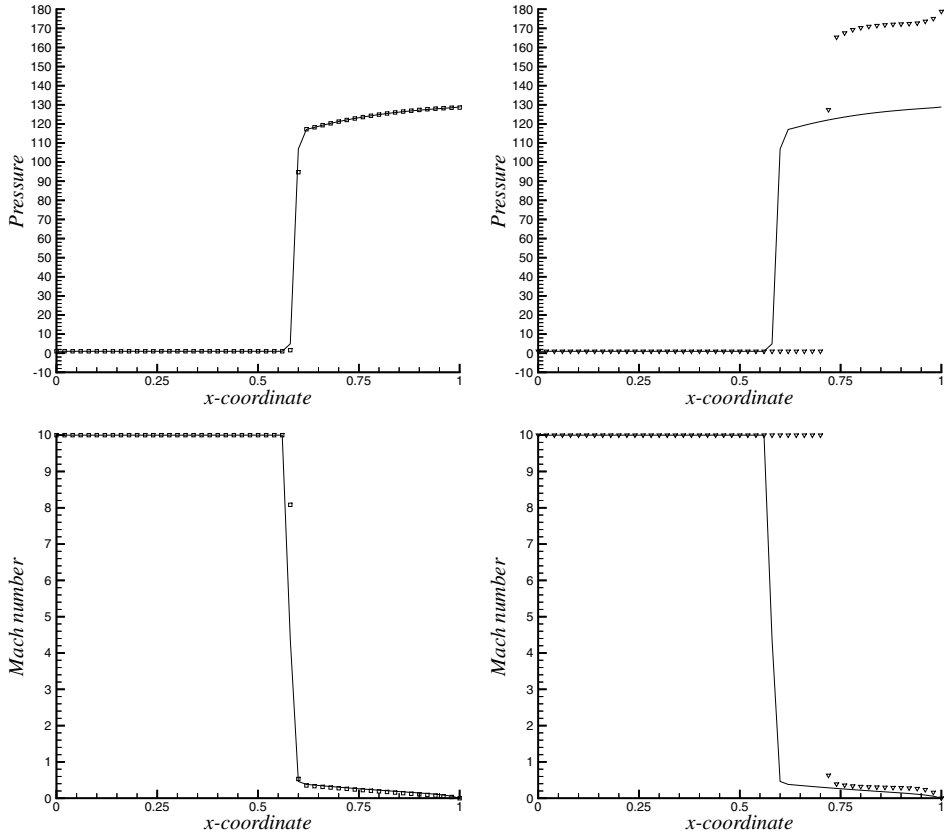

FIG. 7. Mach number and pressure (symbols) along the stagnation line in the Mach 10 bow shock flow around a cylinder computed by the first-order N scheme. Solid line corresponds to the reference solution ($\mathcal{LRD}$ scheme with RSD linearization). (Left) Conservative $\mathcal{CRD}$ scheme. (Right) Standard $\mathcal{LRD}$ scheme combined with the nonconservative linearization in the primitive variables.

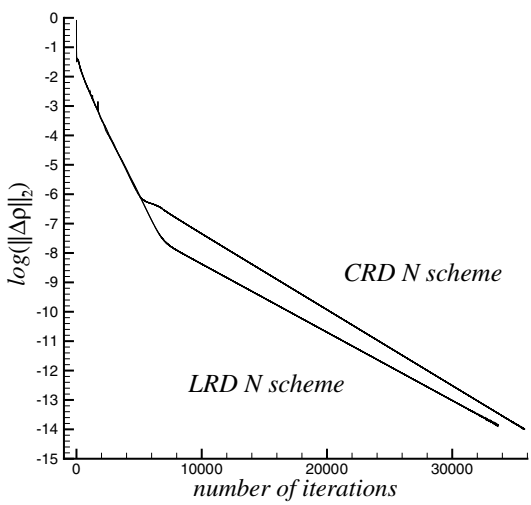

FIG. 8. Convergence histories corresponding to the computation of a Mach 10 bow shock flow around a cylinder obtained by the first-order $\mathcal{LRD}$ and $\mathcal{CRD}$ N schemes.

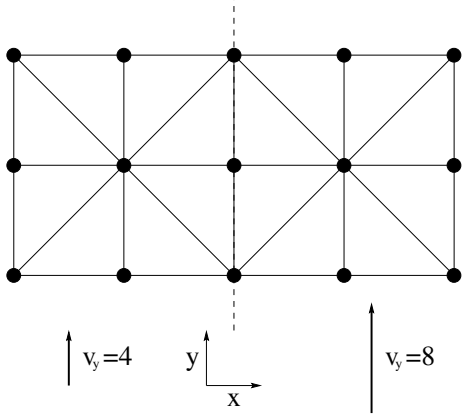

FIG. 9. Schematic view of the structured diamond mesh used in the computation of a contact discontinuity aligned with the mesh, parallel to the y-axes.

The exact solution of this problem is identical to the initial state. However, standard $\mathcal{LRD}$ schemes with RSD linearization modify this equilibrium and converge to a numerical steady state. Results along the outlet (top) boundary are shown for the N scheme in Fig. 10 for three different resolutions. Squares (dotted line), triangles (dashed line), and diamonds (thin solid line) correspond to meshes containing 41×21, 61×31, and 81×41 nodes, respectively. The thick solid line represents the stationary exact solution.

The plots clearly show large perturbations in all primitive variables across the contact. The pressure has a depression which results in the appearance of a force sucking the material toward the interface. Indeed, from the left and right of the interface the x-component of the velocity vector is positive and negative, respectively, indicating a horizontal mass flow toward the center. As a result, the density increases at the interface. The amplitude of the perturbations continuously increases away from the inlet boundary ($y = -0.5$). Computations done with different resolutions demonstrate that the amplitude of the perturbations *increases* as the grid is refined, indicating the instability of the scheme for this particular test case. Obviously, if the resolution is sufficiently high, or if the computational domain is extended in the y-direction, the $\mathcal{LRD}$ schemes yield negative pressure.

However, if the linearization is performed in the set of primitive variables, the $\mathcal{CRD}$ schemes detect and *exactly* preserve the stationary initial solution of this particular flow.

As a next step, we investigate the behavior of the schemes when the initial state *inside* the domain is different from the steady solution. All the numerical experiments are repeated for a strongly perturbed initial state inside the domain while keeping the inlet conditions at the bottom boundary unmodified. The $\mathcal{LRD}$ N scheme shows similar unstable behavior just like before, while the $\mathcal{CRD}$ N scheme converges to a steady state *identical* to the *exact* solution up to machine accuracy.

The problem of the grid-aligned contact discontinuity is also computed by the *LDA* and B schemes. The $\mathcal{LRD}$ *LDA* scheme gives negative pressure before reaching the numerical steady state while the $\mathcal{LRD}$ B scheme introduces oscillations with growing amplitude as the grid is refined, similar to the $\mathcal{LRD}$ N scheme. However, the $\mathcal{CRD}$ *LDA* and B schemes in combination with the linearization in primitive variables preserve the unperturbed stationary initial state and converge to the exact steady state for the case of the perturbed initial state.

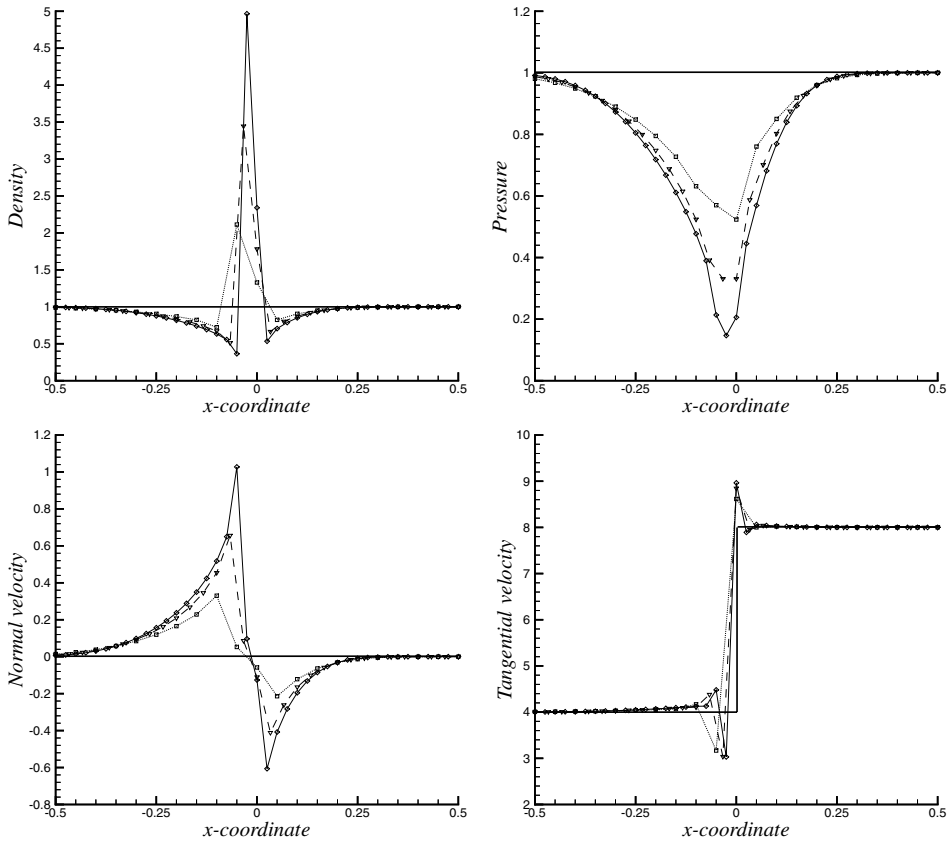

FIG. 10. Solution along the outlet boundary ($y = 0.5$) in the problem of a grid-aligned contact discontinuity computed by the $\mathcal{LRD}$ N scheme. Squares (dotted line), triangles (dashed line), and diamonds (thin solid line) correspond to resolutions of 41, 61, and 81 nodes along the x-axes, respectively. The thick solid line represents the stationary exact solution. Note that the results obtained by the $\mathcal{CRD}$ N scheme are not plotted, since they are identical to the exact solution up to machine accuracy.

We note that the main conclusions obtained so far do not change if the diamond mesh is replaced by a structured grid with left- or right-sided triangles as long as the flow is aligned with the horizontal or vertical edges of the elements. Also, similar effects of instability can be expected not only for the RSD linearization but for some other linearizations as well.

4.4. Rotated Riemann Problem

To investigate the performance of the generalized N scheme for *unsteady* computations, we consider the solution of a rotated Riemann problem over a uniform triangulation of the 2D computational domain containing $n \times 3$ nodes. The rotation angle of the initial interface is $\alpha = \tan^{-1} 0.5$ (see Fig. 11). The top and bottom layers of nodes are connected via shifted periodic boundary conditions. The forward Euler explicit update scheme (13) is employed in combination with a first-order global time-stepping procedure and CFL $= 0.9$.

At $t = 0$ two semiinfinite uniform states are separated by a straight interface (see Fig. 11). In state 1 $\rho_1 = 1$, $v_1^{\perp} = 10$, $v_1^{\parallel} = 0$, and $p_1 = 20$ and in state 2 $\rho_2 = 1$, $v_2^{\perp} = -10$, $v_2^{\parallel} = 0$,

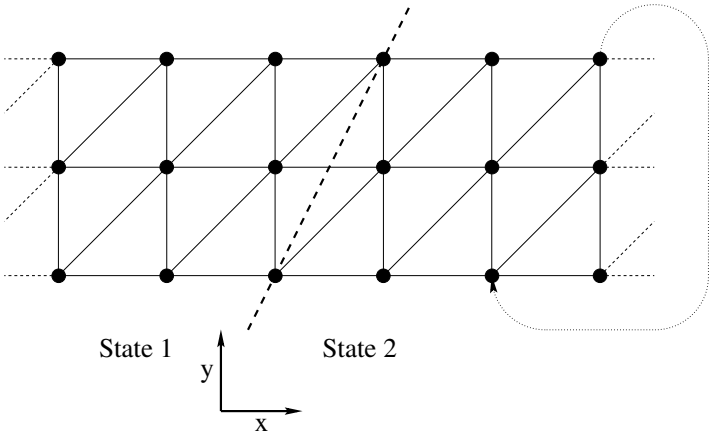

FIG. 11. Schematic view of the grid used in the computation of the rotated Riemann problem. Top and bottom nodes are connected via shifted periodic boundary conditions according to the figure to mimic the infinite extent of the computational domain in the y-direction.

and $p_2 = 1$, where superscript $\perp$ and $\parallel$ refer to the corresponding coordinates of vector quantities in the rotated frame with axes normal and tangential to the initial interface, respectively. The solution of this problem contains a contact discontinuity, and two strong shocks propagating in the opposite directions. The reference computation is performed by a conservative 1D second-order finite-volume code on a fine mesh with $n = 2000$ points employing the Lax–Friedrichs flux function and the *minmod* limiter.

Computational results are shown for the first-order N scheme in Figs. 12 and 13 at $t = 0.15$. The plots at the top, middle, and bottom rows correspond to the conservative $\mathcal{LRD}$ method with RSD linearization, the conservative $\mathcal{CRD}$ method with linearization in primitive variables, and the nonconservative $\mathcal{LRD}$ method with linearization in primitive variables. Numerical results verify the expectations, i.e., the positive conservative schemes gave oscillation-free solutions with proper shock strength and shock speed. However, the $\mathcal{LRD}$ method based on the nonconservative linearization in primitive variables gives a wrong estimation of both the shock strength and the shock speed.

5. APPLICATION TO IDEAL MAGNETOHYDRODYNAMICS

An important application of the presented $\mathcal{CRD}$ schemes is the solution of the set of ideal MHD equations, for which the option of a conservative RSD linearization does not exists. The ideal MHD equations give a fluid approximation of dissipation-free quasineutral plasmas under the presence of external magnetic field. In conservation law form they are written as

$$\frac{\partial}{\partial t}\begin{pmatrix}\rho\\ \rho\mathbf{v}\\ \mathbf{B}\\ E\end{pmatrix}+\nabla\cdot\begin{pmatrix}\rho\mathbf{v}\\ \rho\mathbf{v}\mathbf{v}+\hat{I}P-\mathbf{B}\mathbf{B}\\ \mathbf{v}\mathbf{B}-\mathbf{B}\mathbf{v}\\ \mathbf{v}(E+P)-\mathbf{B}(\mathbf{v}\cdot\mathbf{B})\end{pmatrix}=S, \tag{33}$$

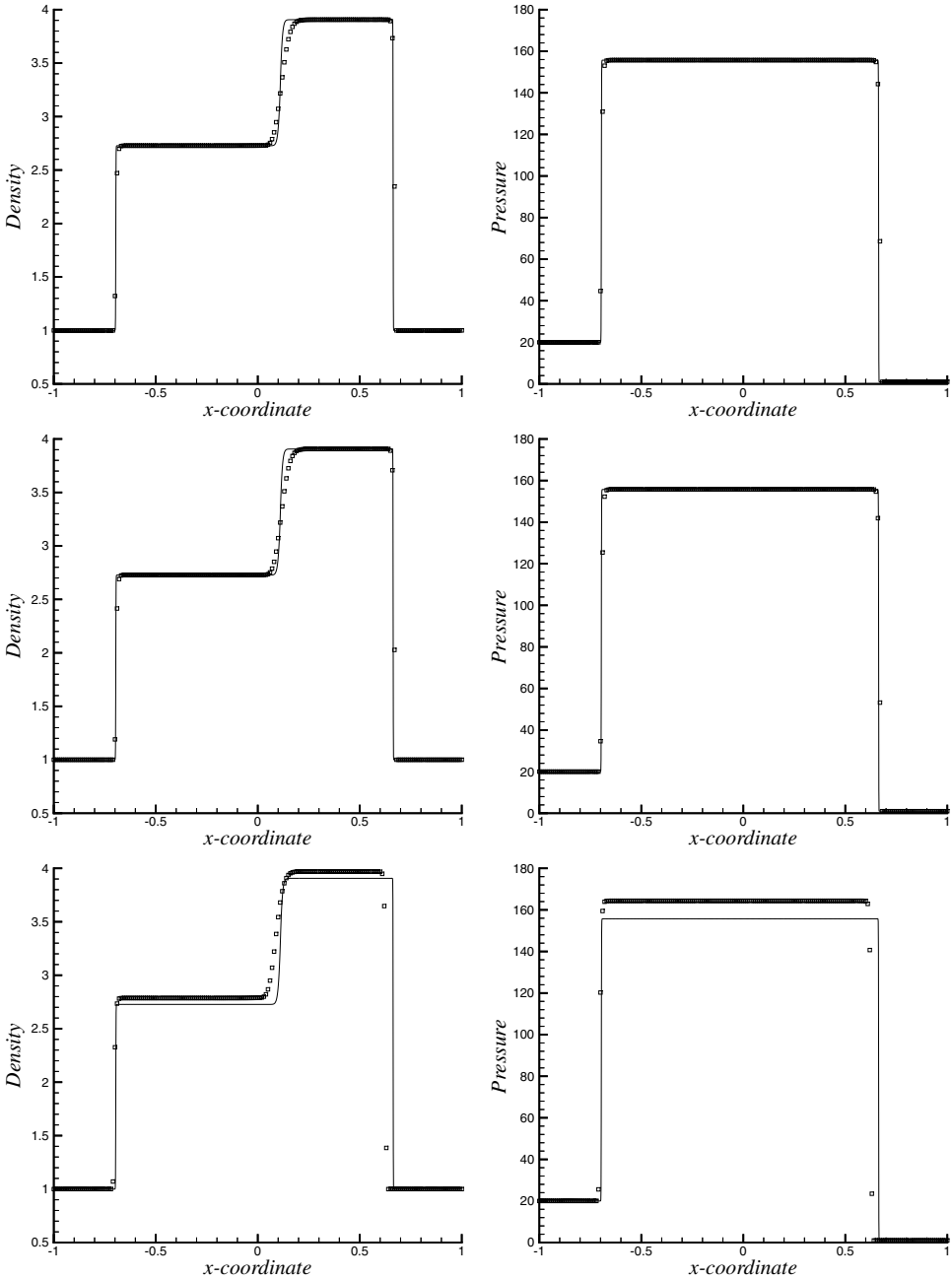

FIG. 12. Rotated Riemann problem on mesh with 201 nodes in the x-direction. Density and pressure are shown at the nodes along the x-axes in the rotated coordinate frame at $t = 0.15$. The solid line represents the reference solution and the symbols correspond to the computed values. (Top row) Standard $\mathcal{LRD}$ scheme with RSD linearization (conservative scheme). (Middle row) New $\mathcal{CRD}$ scheme with linearization in primitive variables (conservative scheme). (Bottom row) Standard $\mathcal{LRD}$ scheme with linearization in primitive variables (nonconservative scheme).

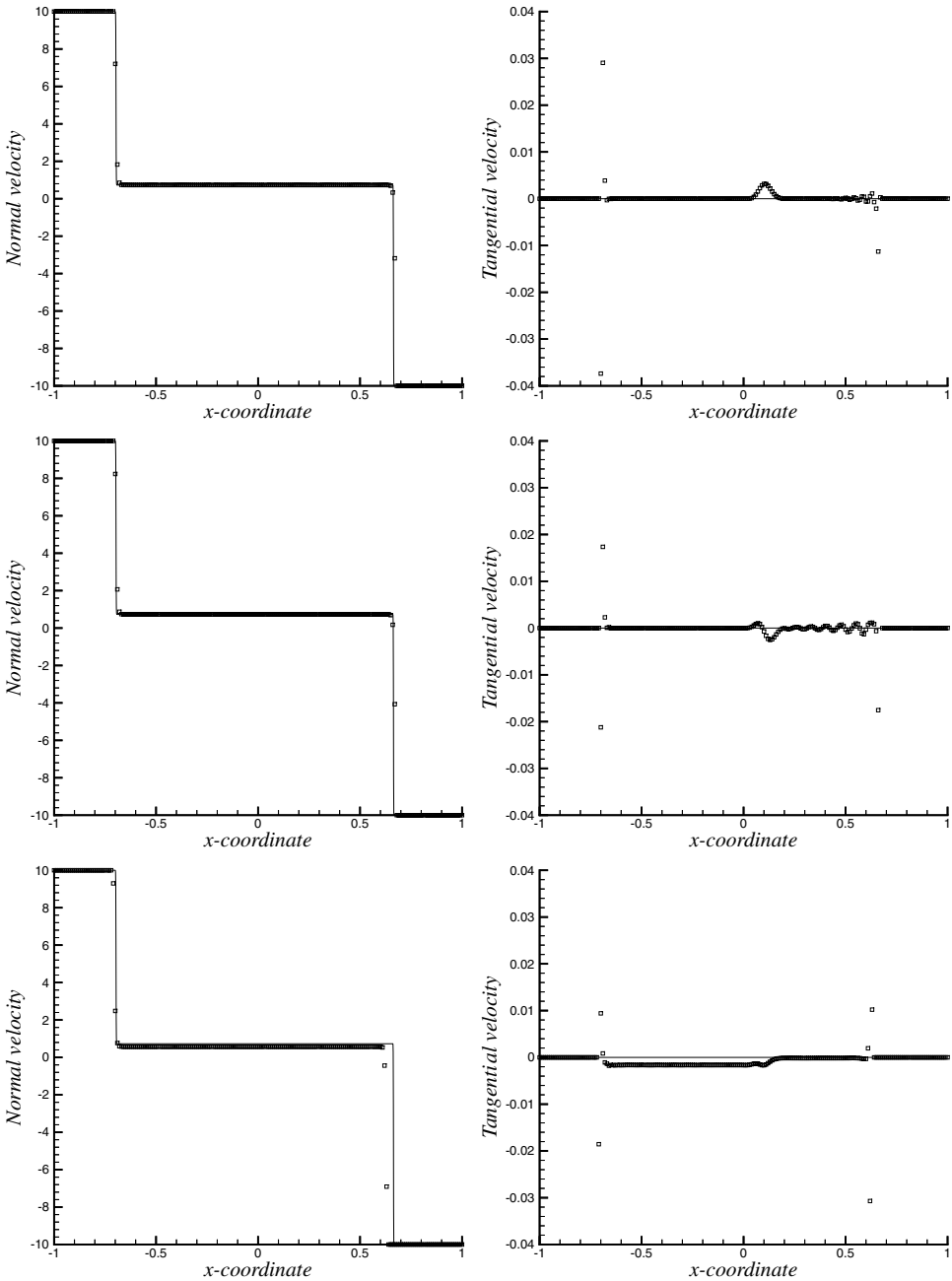

FIG. 13. Rotated Riemann problem on mesh with 201 nodes in the x-direction. Components of the velocity are shown at the nodes along the x-axes in the rotated coordinate frame at $t = 0.15$. The solid line represents the reference solution and the symbols correspond to the computed values. (Top row) Standard $\mathcal{LRD}$ scheme with RSD linearization (conservative scheme). (Middle row) New $\mathcal{CRD}$ scheme with linearization in primitive variables (conservative scheme). (Bottom row) Standard $\mathcal{LRD}$ scheme with linearization in primitive variables (nonconservative scheme).

where $\mathbf{B}$ is the magnetic induction vector, $P = p + \mathbf{B} \cdot \mathbf{B}/2$ is the total pressure, E is the total energy density defined by

$$E = \frac{p}{\gamma - 1} + \frac{1}{2}\rho \mathbf{v} \cdot \mathbf{v} + \frac{1}{2}\mathbf{B} \cdot \mathbf{B}, \tag{34}$$

and S is a source term. In this paper we consider the conservative form obtained by

$$S = \vec{0}, \tag{35}$$

and the nonconservative symmetrizable [12] eight-wave formulation of the ideal MHD equations containing Powell's source term [16],

$$S = -s \nabla \cdot \mathbf{B}, \tag{36}$$

where

$$s = [0, \mathbf{B}, \mathbf{v}, \mathbf{v} \cdot \mathbf{B}]^T. \tag{37}$$

Equation (33) has to be supplemented by the solenoidal condition of the magnetic field, which is merely an initial constraint in an analytic treatment, and maintained all the time if it is initially satisfied:

$$\nabla \cdot \mathbf{B} = 0. \tag{38}$$

There are two main difficulties in the numerical solution procedure of ideal MHD by the $\mathcal{RD}$ method. The first problem concerns the conservation of the convective fluxes. Due to the complexity of the ideal MHD equations the corresponding flux function cannot be written as quadratic functions of any parameter vector, thus precluding the extension of the RSD linearization. In this section we apply the presented $\mathcal{CRD}$ schemes to overcome this difficulty.

The second problem is related to the treatment of the magnetic field. In the course of the numerical solution of the ideal MHD equations the divergence of the magnetic field may deviate from zero, which has a destabilizing effect on a numerical algorithm. Different methods for the special treatment of the magnetic field have been summarized and compared in the framework of finite-volume schemes by Toth [21]. However, the extension of these methods to the context of $\mathcal{RD}$ schemes on unstructured grids turns out to be more complex. In the work of Csík *et al*. [4, 7], the authors considered the symmetrizable [12] eight-wave formulation of the ideal MHD equations containing Powell's source term (36). The inclusion of the source term into the Jacobians regularizes the scheme for multidimensional computations, i.e., removes the singularity from the Jacobians $\partial F_j / \partial U$, and stabilizes against the effect of the nonzero $\nabla \cdot \mathbf{B}$ [4, 7, 16, 17]. However, the nonconservative nature of the source term (36) may lead to wrong jumps across strong shocks [21].

In the present paper matrices K_i^+ and K_i^- are based on the regularized symmetrizable eight-wave formulation of ideal MHD incorporating the so-called divergence wave [16] into the upwinding procedure of the residual. Note that the nonconservative nature of this set of equations forming the basis of the upwinding procedure is unrelated to the conservativity of the cell residual, since in the framework of the $\mathcal{CRD}$ method Φ^E is obtained independently

from K_i. Indeed, if the conservative form of Eq. (33) is solved involving $S = \vec{0}$, then the cell residual is defined by Eq. (15). Concerning the nonconservative cell residual including Powell's source term, Φ^E is computed by

$$\Phi^E = \oint_{\partial E} \mathbf{F}(W^h) \cdot \mathbf{n}\, dS + \int_E s(W^h) \nabla \cdot \mathbf{B}(W^h)\, dV, \tag{39}$$

where the second integral on the right hand side is approximated as

$$\int_E s \nabla \cdot \mathbf{B}\, dV \approx \left(\frac{1}{d+1} \sum_{i=1, i \in E}^{d+1} s_i \right) \left(\frac{1}{d} \sum_{i=1, i \in E}^{d+1} \mathbf{B_i} \cdot \mathbf{n_i} \right). \tag{40}$$

In the simulations the linearization of the Jacobians is done in the set of primitive variables:

$$P_{\mathrm{MHD}} = [\rho, v_x, v_y, B_x, B_y, p]^T. \tag{41}$$

Assuming linear variation of P_{MHD} over an element, formula (40) yields exact integration of the first seven components of Powell's source term; only the last one,

$$\int_E \mathbf{v} \cdot \mathbf{B} \nabla \cdot \mathbf{B}\, dV, \tag{42}$$

corresponding to the energy equation, is integrated approximately.

As an example, we solve the rotated Riemann problem presented in the previous section with the addition of a uniform magnetic field to the initial state. This test case was presented in [8] and also solved by Toth [21] on a 2D mesh to give numerical evidence that finite-volume schemes for the solution of the eight-wave MHD equations with Powell's source term can produce significant errors in the jump relations across strong shocks, and that these errors do not disappear in the limit of vanishing cell size.

At $t = 0$ the two states are given by $\rho_1 = 1$, $v_1^{\perp} = 10$, $v_1^{\parallel} = 0$, $B_1^{\perp} = 5/\sqrt{4\pi}$, $B_1^{\parallel} = 5/\sqrt{4\pi}$, $p_1 = 20$ and $\rho_2 = 1$, $v_2^{\perp} = -10$, $v_2^{\parallel} = 0$, $B_2^{\perp} = 5/\sqrt{4\pi}$, $B_2^{\parallel} = 5/\sqrt{4\pi}$, $p_2 = 1$. The solution of this problem contains a contact discontinuity, a slow shock, a rarefaction wave, and two strong shocks propagating in the opposite directions [8, 21]. Since a conservative RSD linearization does not exist for the ideal MHD equations, we use as reference a conservative 1D second-order finite-volume code on a fine mesh with $n = 2000$ points employing the Lax–Friedrichs flux function and the *minmod* limiter.

The results of the Riemann problem at $t = 0.15$ are shown in Figs. 14–16. The top and middle rows correspond to the conservative treatment of the convective fluxes $\mathbf{F}$ by the $\mathcal{CRD}$ method without and with Powell's source term, respectively. In the bottom row computations based on the linearization in primitive variables combined with the standard definition (19) of W_{in} are shown, including Powell's source term into the Jacobians [4, 7]. Squares indicate the numerical values obtained by the different $\mathcal{RD}$ N schemes on 201 nodes in the x-direction. The continuous line represents the 1D reference solution.

In the analysis of the results we distinguish two different sources of nonconservation error. The first one is due to Powell's source term (36), which vanishes in an analytic treatment, since $\nabla \cdot \mathbf{B} = 0$. This error is only present in the computations shown in the middle and bottom rows. Although it destroys the exact conservation of the fluxes, it adds stability and

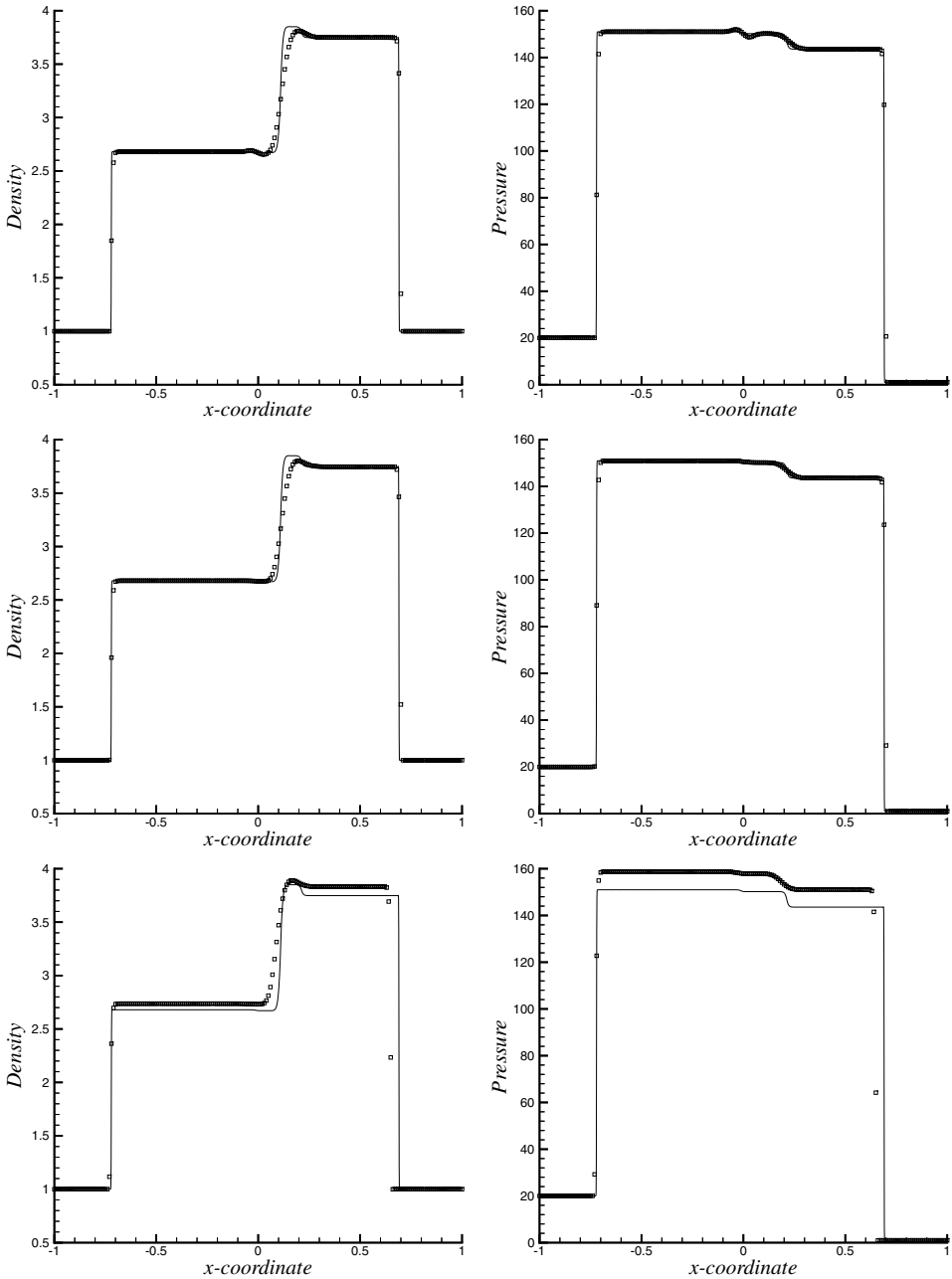

FIG. 14. Rotated MHD Riemann problem on mesh with 201 nodes in the x-direction. Density and pressure are shown at the nodes along the x-axes in the rotated coordinate frame at $t = 0.15$. The solid line represents the reference solution computed by a 1D second-order conservative finite-volume scheme on 2000 points using the Lax–Friedrichs flux function and the *minmod* limiter. Symbols correspond to the computed values. (Top row) $\mathcal{CRD}$ scheme *without* Powell's source term; linearization is done in primitive variables (conservative equation and conservative scheme). (Middle row) $\mathcal{CRD}$ scheme *with* Powell's source term; linearization is done in primitive variables (nonconservative equation and conservative scheme). (Bottom row) $\mathcal{LRD}$ scheme *with* Powell's source term; linearization is done in primitive variables (nonconservative equation and nonconservative scheme).

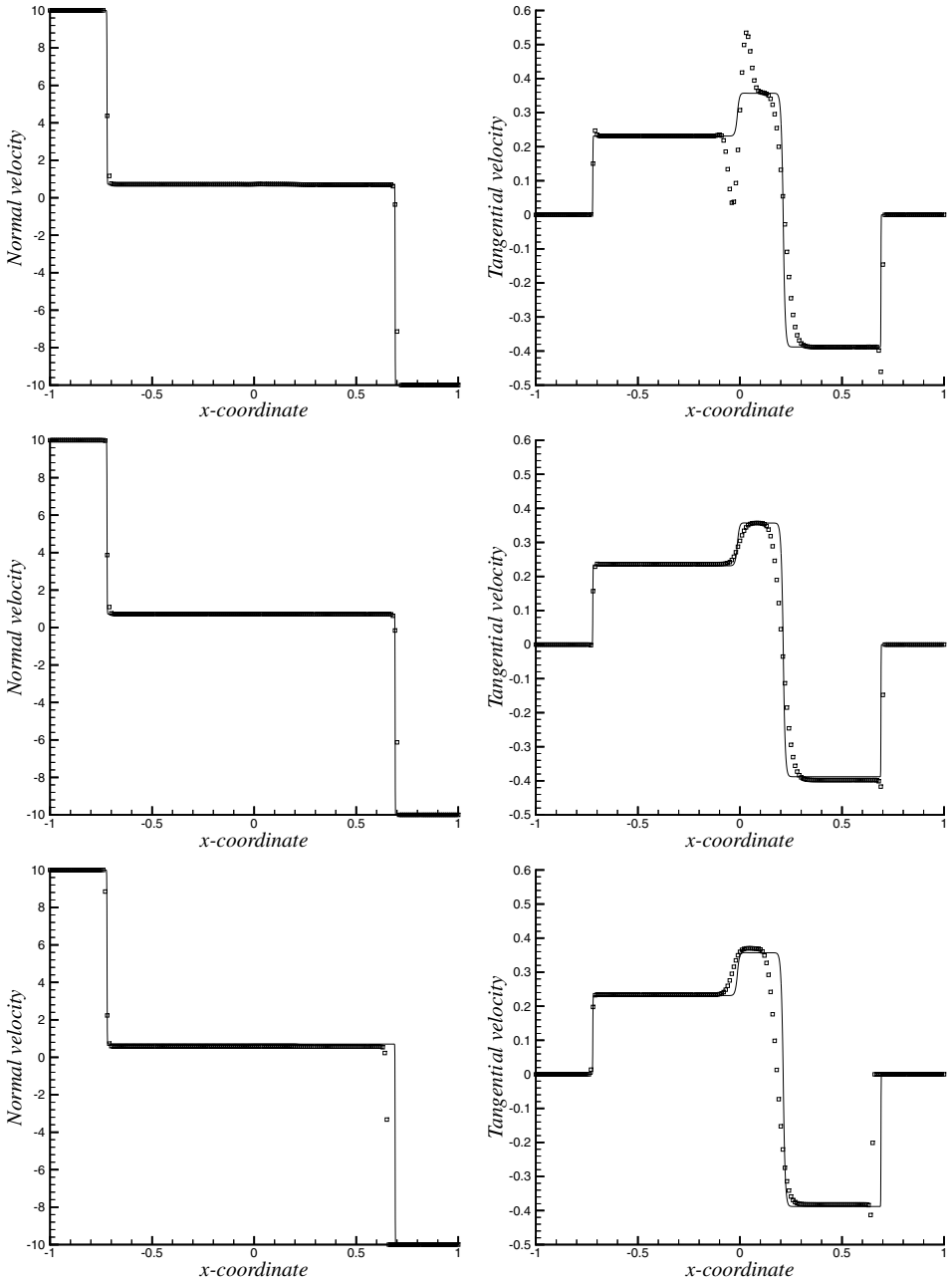

FIG. 15. Rotated MHD Riemann problem on mesh with 201 nodes in the x-direction. Components of the velocity vector are shown at the nodes along the x-axes in the rotated coordinate frame at $t = 0.15$. The solid line represents the reference solution computed by a 1D second-order conservative finite-volume scheme on 2000 points using the Lax–Friedrichs flux function and the *minmod* limiter. Symbols correspond to the computed values. (Top row) $\mathcal{CRD}$ scheme *without* Powell's source term; linearization is done in primitive variables (conservative equation and conservative scheme). (Middle row) $\mathcal{CRD}$ scheme *with* Powell's source term; linearization is done in primitive variables (nonconservative equation and conservative scheme). (Bottom row) $\mathcal{LRD}$ scheme *with* Powell's source term; linearization is done in primitive variables (nonconservative equation and nonconservative scheme).

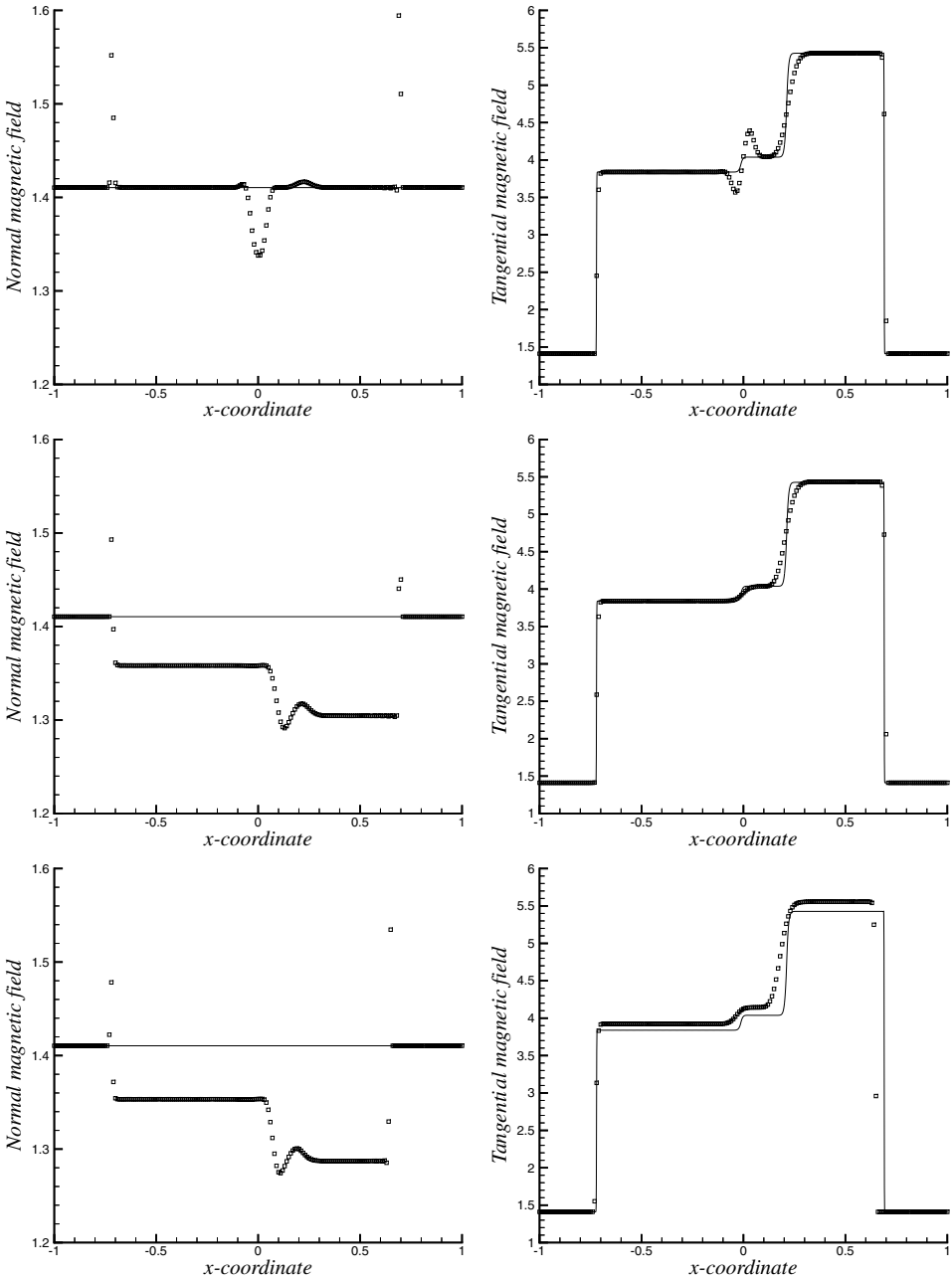

FIG. 16. Rotated MHD Riemann problem on mesh with 201 nodes in the x-direction. Components of the magnetic induction vector are shown at the nodes along the x-axes in the rotated coordinate frame at $t = 0.15$. The solid line represents the reference solution computed by a 1D second-order conservative finite-volume scheme on 2000 points using the Lax–Friedrichs flux function and the *minmod* limiter. Symbols correspond to the computed values. (Top row) $\mathcal{CRD}$ scheme *without* Powell's source term; linearization is done in primitive variables (conservative equation and conservative scheme). (Middle row) $\mathcal{CRD}$ scheme *with* Powell's source term; linearization is done in primitive variables (nonconservative equation and conservative scheme). (Bottom row) $\mathcal{LRD}$ scheme *with* Powell's source term; linearization is done in primitive variables (nonconservative equation and nonconservative scheme).

removes certain errors from the flux function due to the nonzero $\nabla \cdot \mathbf{B}$. Experience has shown that in many cases a computation can be done only with Powell's source term, if no other special treatment for the magnetic field is applied. The second type of nonconservation error is caused by the linearization based on the primitive variables combined with the standard $\mathcal{LRD}$ scheme, which is equivalent to a nonconservative discretization of $\nabla \cdot \mathbf{F}$ in the context of ideal MHD. This error is present only in the computations on the bottom row.

The most significant deviation from the reference solution can be observed in the bottom figures. The shocks propagate with a wrong speed and wrong strength. Compared to the plots in the middle, this feature is mainly attributed to the nonconservative property of the applied $\mathcal{LRD}$ N Scheme. Note that the $\mathcal{CRD}$ scheme *with* the source term closely follows the reference solution on all but one plot. Indeed, the nonconservation error due to Powell's source term is so small in most of the variables that it is hardly visible on the corresponding plots. Surprisingly, the nonconservative nature of Powell's source term gives a significant error only in the normal component of the magnetic field, in agreement with the finite-volume results of Toth [21]. The error is approximately 10%, independent of the resolution (refined computations are not shown).

The fully conservative results for the ideal MHD equations are presented in the top rows. The two strong shocks propagate with the proper speed and proper strength. The solution is monotone across the shocks without spurious oscillations. These observations demonstrate the full conservative property and the positivity of the $\mathcal{CRD}$ schemes applied to ideal MHD. In the right column of Fig. 15, showing the tangential velocity, the reader may observe one or two (depending on the computation) symbols overshooting the reference solution at the position of the shocks. Note that these points correspond to an intermediate solution across the shocks, that they appear to be due to the rotation of 2D vector quantities into the local frame aligned to the initial interface, and that they are unrelated to the monotonicity of the schemes. The same feature is visible, for example, on the right of Fig. 13, showing the tangential velocity for the Riemann problem without the presence of magnetic field solved by the monotone $\mathcal{LRD}$ N scheme.

However, there is an undesired side effect of the full conservativity of the schemes in this particular case. Since large values of $\nabla \cdot \mathbf{B}$ are produced by the multidimensional solution of a 1D problem, significant (and conservative) errors appear in the discrete divergence of the convective fluxes, causing a perturbation of the solution around the initial discontinuity. The fact that these disturbances are not present on the results of the *same* schemes *with* Powell's source term (middle rows) indicate that they are related to the instability due to the nonzero $\nabla \cdot \mathbf{B}$. The main conclusion of this test is that the full conservativity of the first-order linear monotone N scheme in the context of ideal MHD is obtained by the application of the $\mathcal{CRD}$ method; however a robust treatment for the discretization of the magnetic field is still needed.

6. CONCLUSIONS

In the present paper we propose a new formulation of the positive $\mathcal{RD}$ N scheme based on the conservative contour integral of the convective fluxes. By construction, this scheme is conservative for *arbitrary* flux functions and does not require the existence of an exact RSD linearization. Instead, the linearization of the Jacobian matrices can be based on physical reasonings, consideration of simplicity, and low computational cost. In the present paper we employ a linearization based on the primitive variables, which is cheap to compute.

According to the experience of the authors the new $\mathcal{CRD}$ N scheme is extremely robust and reliable even for very strong normal shocks. Moreover, it retains the accuracy and good convergence property of the original $\mathcal{LRD}$ schemes.

The benefit of the new $\mathcal{CRD}$ schemes may be considerable already in applications for the Euler equations, where an exact conservative RSD linearization exists. As an example, in the presence of strong grid-aligned shear flows the RSD linearization is known to introduce a large pressure gradient across the shear, rendering $\mathcal{LRD}$ schemes inaccurate and unstable. If the linearization is performed in the set of primitive variables defined before, the problem does not appear in combination with the new $\mathcal{CRD}$ schemes; grid-aligned shear flows stay stable. Our computations indicate that in certain cases the robustness of the $\mathcal{LRD}$ and $\mathcal{CRD}$ B schemes is not satisfactory, especially for high-Mach-number flows expressing the need for an improved nonlinear monotone $\mathcal{RD}$ scheme.

The most important applications of the new $\mathcal{CRD}$ schemes probably concern the solution of highly nonlinear conservation laws where an exact RSD linearization does not exist, such as the equations describing ideal magnetohydrodynamics, two-phase flows, or chemically reacting space reentry flows.

As an example the $\mathcal{CRD}$ schemes were applied to the solution of the ideal magnetohydrodynamics equations. Numerical results confirm the conservativity and positivity of the method across strong unsteady shocks. We also pointed out that a robust and conservative treatment of the magnetic field is still needed.

Another potential application of the presented $\mathcal{CRD}$ approach concerns the extension of the $\mathcal{RD}$ method to the context of nonlinear finite-element representation of the solution. These elements can be, for example, cubic elements on triangles or complete finite elements on 2D quadrilaterals and 3D hexahedra. Just as in the case of highly nonlinear conservation laws on linear elements, the RSD linearization does not extend to these nonlinear finite elements either. An elegant way to ensure the conservative property of the monotone $\mathcal{RD}$ schemes for nonlinear finite elements could be the employment of the $\mathcal{CRD}$ method. These ideas will be explored in the future.

REFERENCES

1. R. Abgrall, Toward the ultimate conservative scheme: Following the quest, *J. Comput. Phys.* **167**, 277 (2001).
2. R. Abgrall and T. J. Barth, Residual distribution schemes for conservation laws via adaptive quadrature, submitted for publication.
3. D. Caraeni, M. Caraeni, and L. Fuchs, *A Parallel Multidimensional Upwind Algorithm for LES*, AIAA Paper 2001-2547 (AIAA Accession number 31057) (2001).
4. Á. Csík, H. Deconinck, and S. Poedts, *Monotone Residual Distribution Schemes for the Ideal 2D Magnetohydrodynamic Equations on Unstructured Grids*, AIAA Paper 99-3325 (AIAA Accession number 33525) (1999).
5. Á. Csík and H. Deconinck, Space time residual distribution schemes for hyperbolic conservation laws on unstructured linear finite elements, in *Numerical Methods for Fluid Dynamics VII*, edited by M. J. Baines, Oxford University Computing Laboratory, Oxford (2001). p. 557.
6. Á. Csík, M. Ricchiuto, H. Deconinck, and S. Poedts, *Space-Time Residual Distribution Schemes for Hyperbolic Conservation Laws*, AIAA Paper 2001-2617 (AIAA Accession number 31161) (2001).
7. Á. Csík, H. Deconinck, and S. Poedts, Monotone residual distribution schemes for the ideal magnetohydrodynamic equations on unstructured grids, *AIAA J.* **39**(8), 1532 (2001).
8. W. Dai and P. R. Woodward, An approximate riemann solver for ideal magnetohydrodynamics, *J. Comput. Phys.* **111**, 354 (1994).

9. H. Deconinck, P. L. Roe, and R. Struijs, A multidimensional generalization of Roe's flux difference splitter for the Euler equations, *Comput. Fluids* **22**, 215 (1993).
10. H. Deconinck, K. Sermeus, and R. Abgrall, *Status of Multidimensional Upwind Residual Distribution Schemes and Applications in Aeronautics*, AIAA Paper 2000-2328 (AIAA Accession number 33804) (2000).
11. E. van der Weide, H. Deconinck, E. Issmann, and G. Degrez, Fluctuation splitting schemes for multidimensional convection problems: An alternative to finite volume and finite element methods, *Comput. Mech.* **23**(2), 199 (1999).
12. S. K. Godunov, *Symmetric Form of the Equations of Magnetohydrodynamics* (translated by Timur Linde), available at http://hpcc.engin.umich.edu/CFD/publications/publications.html.
13. A. Jameson, *Artifical Diffusion, Upwind Biasing, Limiters and Their Effect on Accuracy and Multigrid Convergence in Transonic and Hypersonic Flows*, AIAA Paper 1993-3359 (1993).
14. H. Nishikawa, M. Rad, and P. L. Roe, *A Third-Order Fluctuation Splitting Scheme That Preserves Potential Flow*, AIAA Paper 2001-2595 (AIAA Accession number 31156) (2001).
15. H. Paillére, *Multidimensional Upwind Residual Distribution Schemes for the Euler and Navier–Stokes Equations on Unstructured Grids*, Ph.D. thesis (Université Libre de Bruxelles, Belgium, 1995).
16. K. G. Powell, P. L. Roe, R. S. Myong, T. I. Gombosi, and D. L. De Zeeuw, *An Upwind Scheme for Magnetohydrodynamics*, AIAA Paper 1995-1704 (1995).
17. K. G. Powell, P. L. Roe, T. J. Linde, T. I. Gombosi, and D. L. De Zeeuw, A solution-adaptive upwind scheme for ideal magnetohydrodynamics, *J. Comput. Phys.* **154**, 284 (1999).
18. M. Rad and P. L. Roe, An Euler code that can compute potential flow, in *Finite Volumes for Complex Applications II–Problems and Perspectives*, edited by R. Vilsmeier, F. Benkhaldoun, D. Hanel, proceedings published by Hermes, Duisberg, Germany (1999).
19. P. L. Roe and H. Nishikawa, Adaptive grid generation by minimising residuals, in *Numerical Methods for Fluid Dynamics VII*, edited by M. J. Baines, Oxford University Computing Laboratory, Oxford, p. 45 (2001).
20. R. Struijs, *A Multi-Dimensional Upwind Discretization Method for the Euler Equations on Unstructured Grids*, Ph.D. thesis (University of Delft, The Netherlands, 1994).
21. G. Toth, The $\nabla \cdot B = 0$ constraint in shock-capturing magnetohydrodynamics codes, *J. Comput. Phys.* **161**, 605 (2000).